Correlation between physicochemical properties of superparamagnetic iron oxide nanoparticles and their reactivity with hydrogen peroxide

Taraneh Javanbakht*[1], Sophie Laurent[2,3], Dimitri Stanicki[2], Mathieu Frenette[1]

[1]Department of Chemistry, Université du Québec à Montréal, Montreal, Quebec, Canada H2X 2J6

[2]Laboratory of NMR and Molecular Imaging, University of Mons, Avenue Maistriau 19, B-7000 Mons, Belgium

[3]Center for Microscopy and Molecular Imaging (CMMI), 6041 Gosselies, Belgium

*Corresponding author: Taraneh Javanbakht

email: taraneh.javanbakht@uqam.ca

ABSTRACT

The present study focuses on the effects of the physicochemical properties of superparamagnetic PEG-modified, positively charged and negatively charged iron oxide nanoparticles (SPIONs) on their reactivity with hydrogen peroxide. Our hypothesis was that the reactivity of SPIONs in this reaction would depend on their surface properties. The comparative study of the nanoparticles with DLS and TEM revealed the average sizes of PEG-modified, positively charged and negatively charged SPIONs. We observed that the reactivity of negatively charged SPIONs with hydrogen peroxide was less than that of positively charged SPIONs and that of these second nanoparticles was less than that of PEG-modified SPIONs. This difference in the reactivity of these SPIONs with hydrogen peroxide was attributed to the presence of carboxyl or amine groups on their surface. However, the values of the rate constants of the reactions of PEG-SPIONs, positively charged SPIONs and negatively charged SPIONS with hydrogen peroxide showed that the reaction of negatively charged SPIONs with hydrogen peroxide was more rapid than that of PEG-SPIONs and the reaction of this second SPIONs with hydrogen peroxide was more rapid than that of positively charged SPIONs. The surface study of the SPIONs using XPS showed that the high resolution spectra of these nanoparticles changed after reaction with hydrogen peroxide, which indicates their surface modifications. These investigations can help develop more appropriate nanoparticles with controlled physicochemical properties.

Keywords: superparamagnetic iron oxide nanoparticles, FTIR, DLS, SEM, XPS, oxygen uptake

INTRODUCTION

The surface modification of nanoparticles has attracted significant interest over the last decades. Nanoparticles consist of a core and shell with dimensions of 1-100 nm that results in different physicochemical properties than those of lager particles.[1] The high reactivity of nanoparticles is due to their large surface to volume ratio.[2]

Superparamagnetic iron oxide nanoparticles (SPIONs) are nanoparticles with a variety of biomedical applications such as magnetic resonance imaging (MRI), tissue engineering, drug delivery, etc.[3-6] During the recent years, the biomedical applications of the nanocomposites of polyethyleneglycol (PEG) with superparamagnetic iron oxide nanoparticles (SPIONs) have been investigated. The biocompatibility of SPIONs is increased with this polymer for these applications.[7,8] PEG is a polar organic polymer that is used for the coating of nanoparticles.[9,10] The coating of SPIONs with PEG is performed either by refluxing at high temperature,[11] coating with oleic acid or recoating with PEG,[12] etc. The coating of SPIONs includes *in situ* coating, post-synthesis adsorption and post-synthesis end grafting.[13] The incorporation of SPIONs to PEG can be carried out via either the encapsulation of nanoparticles within the polymer or their infiltration into it during swelling.[6]

Iron and hydrogen peroxide are oxidizing agents. The oxidation of organic compounds with hydrogen peroxide in the Fenton reaction was first described by H.J.H. Fenton who observed the oxidation of tartaric acid by hydrogen peroxide in the presence of ferrous iron ions. This reaction includes a mixture of hydrogen peroxide and ferrous iron is currently accepted as one of the most effective methods for the oxidation of organic pollutants.[14] The Fenton reaction is capable of generating both hydroxyl radicals and higher oxidation states of the iron has been studied previously.[15] It is worth noting that during the peroxidation, the autoxidation of the reagent can generate hydroxyl radicals from a secondary oxidation mechanism.[16] The surfaces of iron oxide nanoparticles are capable of catalytically generating reactive oxygen species (ROS) through the Fenton reaction.[17] It has been also confirmed that this reaction is effective in treating various industrial waste water components including aromatic amines, a wide variety of dyes, pesticides, surfactants, explosives as well as many other substances.[14] The comparative surface modification of PEG-modified and functionalized SPIONs with hydrogen peroxide has not been studied,

yet. Moreover, the reactivity of SPIONs with hydrogen peroxide has not been related to the physicochemical properties of these nanoparticles.

In this paper, for the first time the reactivity of PEG-coated, positively and negatively charged SPIONs with hydrogen peroxide has been studied. The surface properties of these nanoparticles were correlated with their reactivity with hydrogen peroxide. The relation between the surface charge and other physicochemical properties of SPIONs with this issue has also been studied.

Figure 1 shows the structure of TPED-modified and TEPSA-modified SPIONs. The PEG-modified SPIONs are TEPSA-modified SPIONs with PEG coating around carboxyl groups.

Figure 1: The structure of TPED-modified and TEPSA-modified SPIONs. The violet circle and blue shell around it represent the core of magnetite nanoparticles and their silica coating. X in the $C(H_2)_n$ functional groups on the surface of nanoparticles represents either amine or carboxyle in positively or negatively charged SPIONs, respectively.

MATERIALS AND METHODS

Chemicals

For the synthesis of SPIONs, these chemicals were used: methanol HPLC purchased from ChemLab, acetone (ACS reagent, ≥99.0%), diethylic ether (ACS reagent, ≥99.0%), dimethylformamide anhydrous HPLC-grade, n-[3-(trimethoxysilyl)propyl] ethylenediamine (TPED) (97%), all purchased from Sigma-Aldrich. Diethylene glycol (DEG, > 99%) and iron (II) chloride tetrahydrated (99%) were both purchased from Merck. A solution of iron (III) chloride (45%) was purchased from Riedel-de Haën. 1-ethyl-3-(3-dimethylaminopropyl) carbodiimide (EDC, >98%) and tetramethylammonium hydroxide (>95%) were purchased from TCI Chemicals. 3-(triethoxysilyl)propyl succinic anhydride (TEPSA) (>94%) was purchased from ABCR. Hydrogen peroxide (30% w/v), monopotassium phosphate, dipotassium phosphate, nitric acid, and sulfuric acid were purchased from Sigma-Aldrich.

Synthesis of iron oxide cores

Magnetite nanoparticles (NPs) were prepared by co-precipitation of iron salts in DEG according to a protocol previously described.[19] Briefly, 8.9 g of ferrous chloride

tetrahydrate salt (45 mmol) and 9.1 ml ferric chloride (45%; 37 mmol) in DEG (250 ml) were heated at 170°C. After 15 min, 15 g of solid sodium hydroxide was added in order to prevent any dilution. After stiring the solution for 1 h at 170°C, the mixture was cooled and the magnetic particles were isolated from the solution and washed with an aqueous solution of nitric acid (200 ml, 1 M). Finally, magnetite was dispersed in deionized water, sonicated for 45 minutes and centrifuged at 16 500g for 45 min to remove aggregates.

Preparation of PEG-modified nanoparticles

After adding O-(2-aminoethyl)-O'-methyl-polyethyleneglycol (120 mmol; 90 mg) to TEPSA-modified ferrofluid (150 mM in iron; 5 ml) in the presence of EDC (200 mmol; 38 mg), the pH was adjusted to 7.5. Then, the mixture was stirred at room temperature. After 15 hours of reaction, the suspension was purified by filtration using a membrane with cut-off : 30 kDa.

Preparation of TPED-modified nanoparticles (positively charged SPIONs)

N-[3-(trimethoxysilyl)propyl] ethylene-diamine (TPED) was grafted to the nanoparticles. This was done by adding TPED (25 mmol; 5.4 mL) to a suspension of nanoparticles in nitric acid (100 mL, [Fe] = 25 mM) at 50°C. The suspension was stirred for 2 h under boiling conditions and the mixture was cooled to room temperature. Then, the suspension was purified by filtration sing a membrane with cut-off : 30 kDa. Finally, it was centrifuged at 16 500 g for 45 minutes.

Preparation of TEPSA-modified magnetic nanoparticles (negatively charged SPIONs)

In a first step, the suspension of NPs (20 ml; [Fe] 1⁄4 250 mM) was diluted with dimethylformamide (50 ml). Then, water was eliminated. TEPSA (25 mmol; 7.1 ml) was added to the nanoparticle dispersion in DMF. The addition of water (4.3 ml) was followed by an aqueous solution of TMAOH (1 M; 2.5 mmol; 2.5 ml) at room temperature and under stirring. After heating the solution at 100 °C for 24 h, the magnetic nano-objects were collected. After pouring the suspension in an acetone/diethylether mixture (50/50) and magnetic decantation, it was washed with acetone. Then, the black precipitate was dispersed in water and purified by filtration using a membrane with cut-off: 30 kDa. Finally, it was centrifuged at 16 500 g for 45 minutes.

We reported the surface charge of TPED-modified and TEPSA-modified SPIONs in our previous works.[18,19] In the current work, the preparation of PEG-modified nanoparticles was aimed to neutralize the surface charge of NPs in TEPSA-modified ferrofluid.[20]

Fourier Transform Infrared (FTIR) Spectroscopy

Using a Perkin Elmer spectrum 65 FTIR spectrometer, attenuated total reflectance was measured on a diamond surface in the range of 600-4000 cm^{-1}. FTIR spectra at 4 cm^{-1} resolution were recorded with 32 averaged scans to improve S/N.[21]

Dynamic Light Scattering (DLS)

The particle size distribution of the SPIONs was measured in aqueous suspensions using dynamic light scattering (DLS) (Malvern Zetasizer Nano ZS).[22] Samples were sonicated prior to analysis. Scattered light was measured at different angles at room temperature. Intensity distributions were converted into volume and number distributions in order to obtain mean sizes. Means and standard deviations were obtained from three replicate measurements.

Transmission electron microscope (TEM)

A transmission electron microscope (TEM) JOEL JEM 2100F was used to image the samples.[23] Gatan Digital Micrograph software was used for the analysis of the TEM images. Average sizes of the SPIONs were calculated on the basis of fifty SPIONs for each sample.

Measurement of reactivity with hydrogen peroxide

The reactivity of the neutral, positively charged and negatively charged SPIONs with H_2O_2 was measured with a TECAN infinite M1000 PRO microplate reader. The i-control 1.9 software was used for the acquisition of data. The reaction mixtures (0.3 mL) were composed of 0.16 mM SPIONs, H_2O_2 3%, and 60 mM phosphate buffer without NaCl, pH 7.0, at room temperature.

The reaction was monitored by measuring the absorbance at 350 nm.[24] QtiPlot 0.9.8.9 was used for curve fitting and the apparent reaction constants were calculated for the reactions of SPIONs with hydrogen peroxide. The below equation was used for the calculations of these data:

$$y = y_0 + A * \exp(-x / t)$$

The curves were obtained from the data of the nanoparticles in dispersion.

Titration of samples

The titration of hydrogen peroxide in the samples of SPIONs after reaction in phosphate buffer as well as that of hydrogen peroxide without SPIONs as control were carried out with potassium permanganate. First, the titer of potassium permanganate was determined with a titration with sodium oxalate. The sodium oxalate was weighted in a beaker on a balance. Then, the standard substance was diluted with 50 mL of 5% sulphuric acid solution and heated on a mixer heater to 70°C, because the titration reaction was too slow at room temperature.[25]

The equivalent point was reached with a titration as soon as the colour of the solution turned permanently light pink in the presence of potassium permanganate. The second titration was done with potassium permanganate to determine the concentrations of hydrogen peroxide in the samples. The same procedure as the first titration was carried out but the solution samples were not heated in the second titration. The samples were 100 times diluted in millipore water and the concentrations of hydrogen peroxide were calculated considering the dilution factor.

Inductively couples plasma atomic emission spectroscopy (ICP-OES) analysis of iron in samples

An Agilent Technologies 5100 ICP-OES equipped with the ICPExpert software was used to measure the amount of iron in samples of SPIONs after reaction with hydrogen peroxide.[26] The standard solution were used for the calibration of equipment before the quantification of iron in samples.

The concentrations of iron in the blank (nitric oxide 5%), the calibration solutions and samples were measured at the wavelengths of 234.4 nm, 238.2 nm, 259.9 nm and their average data were calculated.

X-Ray Photoelectron Spectroscopy (XPS)

XPS analysis was conducted with a collecting survey of C1s, O1s, and N1s high-resolution spectra of both treated and untreated CNCs on a VG ESCALab 3 Mk II, using non-monochromated Mg Kα radiation (1253.6 eV), at a power setting of 300 W. The instrument resolution was 0.7 eV. Samples were deposited onto silica substrates, using two-sided adhesive Cu tape. The base pressure during scanning was 1×10^{-9} torr. Electrons were

detected at a perpendicular takeoff angle, using 0.05 eV steps, and spectra were analyzed using the VG Avantage software package.[27]

RESULTS AND DISCUSSION

FTIR analysis of the SPIONS. Figure 2 shows the FTIR spectra of the PEG-modified SPIONs, positively charged SPIONs and negatively charged SPIONs before and after reaction with hydrogen peroxide and phosphate buffer.

Figure 2: FTIR spectra of the (a,d) PEG-modified, (b,e) positively charged, (c,f) negatively charged SPIONs before and after reaction with hydrogen peroxide and (g) phosphate buffer.

The peaks at 1000 cm^{-1} and 1330 cm^{-1} are attributed to C-Ostretching (Fig. 2a, 2b, 2c). The silica shell on the surface of positively and negatively charged SPIONs Si-O stretching bond was visible in the peak at 1100 cm^{-1} (Fig. 2a, 2b, 2c).[28] The peak that appears near 1660 cm^{-1} in the spectrum of positively charged SPIONs corresponds to the amine bending mode[29] (Fig 2b), whereas the peaks at 1555 cm^{-1} and 1420 cm^{-1} can be attributed to asymmetric and symmetric stretching of carboxyl group.[30]

In general, the spectra appear to lose fine structure following hydrogen peroxide treatment (Fig. 2d, 2e, 2f) with the peaks that correspond to those of phosphate buffer (Fig. 2g). This indicates that after reaction with hydrogen peroxide, only the buffer was present in the samples.

DLS analysis

We measured the average sizes of PEG-modified, positively charged and negatively charged SPIONs with DLS analysis.

The average sizes of PEG-modified, positively charged and negatively charged SPIONs were 19.3 ± 0.1 nm, 30.6 ± 0.1 nm and 15.7 ± 0.2 nm respectively. The size variations correspond to the standard deviations of three measurements for each sample. The bigger size of positively charged SPIONs may be due to the aggregation of these nanoparticles.

TEM imaging. Figure 3 shows the TEM images of the a) PEG-modified, b) positively and c) negatively charged SPIONs.

Figure 3: Representative TEM images of the a) PEG-modified, b) positively and c) negatively charged SPIONs.

The average sizes of PEG-modified, positively charged and negatively charged SPIONs were 7.8 ± 2.0 nm, 6.4 ± 1.5 nm and 8.1 ± 1.4 nm respectively. The average silica coating of SPIONs was roughly 1 nm.

Table 1 presents the size values of SPIONS measured with DLS and TEM.

Table 1: The size values of SPIONS measured with DLS and TEM.

Analysis method	PEG-modified SPIONs	positively charged SPIONs	negatively charged SPIONs
DLS	19.3 ± 0.1 nm	30.6 ± 0.1 nm	15.7 ± 0.2 nm
TEM	7.8 ± 2.0 nm	6.4 ± 1.5 nm	8.1 ± 1.4 nm

Measurements of reactivity with hydrogen peroxide

Figure 4 shows the reactivity of PEG-modified SPIONs, positively charged SPIONs and negatively charged SPIONs with hydrogen peroxide.

As shown in Figure 4, the negatively charged SPIONs show a less pronounced decrease in absorbance at 350 nm with hydrogen peroxide than the positively charged SPIONs and PEG-SPIONs. This may be due to the negative surface charge of these nanoparticles that can prevent hydrogen peroxide to attack their surface. The comparison of these two last nanoparticles reveals that PEG-SPIONs have the most reactivity with hydrogen peroxide than the positively charged SPIONs. This may be due to the presence of the positive surface charge of the nanoparticles that makes them resist more resistant to hydrogen peroxide than PEG-SPIONs that are deprived of surface charge.

Figure 4: Normalized absorbance at 350 nm of PEG-modified, positively charged and negatively charged SPIONs following their reaction with 3% hydrogen peroxide.

The apparent decay rate constantsrates of the reactions of PEG-SPIONs, positively charged SPIONs and negatively charged SPIONS SPIONs in 3% hydrogen peroxide were $1.1*10^{-2}$ min^{-1}, $8.2*10^{-3}$ min^{-1} and $2.9*10^{-2}$ min^{-1}, respectively.

Titration of samples

Following reactions between SPIONs and hydrogen peroxide, the residual amount of hydrogen peroxide was determined by permanganate titration. In all cases, the residual hydrogen peroxide was minimal (< 0.005%) indicating its complete decomposition by the SPIONs.

ICP-OES analysis of iron in samples

Figure 5 shows the percentage of iron concentrations in the supernatant solution of centrifuged SPIONs before and after the reaction with hydrogen peroxide.

Figure 5: The percentage of iron concentrations in the samples before and after the reaction with hydrogen peroxide

As seen in Figure 5, the concentration of iron in the samples of PEG-modified, positively charged and negatively charged SPIONs did not change after reaction with hydrogen peroxide in comparison with those samples before the reaction. This can be due to the protection of this metal in the core of nanoparticles from peroxide attack because of coating nanoparticles with PEG in the first samples or their surface functionalization in the other ones.

XPS measurements

Figure 6 shows the XPS O1s high resolution spectra of (a,b) PEG-modified, (c,d) positively and (e,f) negatively charged SPIONs before and after reaction with hydrogen peroxide.

Figure 6: The XPS O1s high resolution spectra of (a,b) PEG-modified, (c,d) positively and (e,f) negatively charged SPIONs before and after reaction with hydrogen peroxide.

In the survey spectra of samples before and after reaction with hydrogen peroxide, oxygen, iron, carbon, nitrogen and silicon peaks were observed (data not shown). In the XPS O1s high resolution spectra, the peaks at 529.5 eV (and in some peaks 530 eV), 531 eV (and in some peaks 531.5 eV) and 532.5 eV (and in some peaks 533 eV) correspond to O-Fe, O-H and O-Si bonds, respectively. The decrease in the intensity of peaks was attributed to the reaction of SPIONs with hydrogen peroxide.

Table 2 presents the ratios of the XPS peak intensities of SPIONs before and after reaction with hydrogen peroxide.

Table 2: The ratios of the XPS peak intensities of SPIONs before and after reaction with hydrogen peroxide.

Ratio of peak intensities	PEG-modified SPIONs	Positively charged SPIONs	Negatively charged SPIONS
O-Fe	5.0	5.8	3.1
O-H	2.2	2.3	2.4
O-Si	1.5	3.7	2.1

Figure 7 shows the percentage change of iron and oxygen at the surface of PEG-modified SPIONs, positively charged SPIONs and negatively charged SPIONs before and after reaction with hydrogen peroxide.

Figure 7: The percentage change of a) oxygen and b) iron at the surface of 1) PEG-modified SPIONs, 2) positively charged SPIONs and 3) negatively charged SPIONs before and after reaction with hydrogen peroxide.

As seen in Figure 7, the percentage of oxygen was more at the surface of the negatively charged SPIONs in comparison with the positively charged SPIONs and it was more at the surface of the positively charged SPIONs in comparison with the PEG-modified SPIONs. The same difference was observed for the percentage of iron among the SPIONs. It was also observed that the percentage of oxygen and iron at the surface of the PEG-modified SPIONs, the positively charged SPIONs and the negatively charged SPIONs decreased after reaction with hydrogen peroxide. The least amount of the percentage of oxygen was observed at the surface of negatively charged SPIONs, more amount of oxygen was observed for the positively charged SPIONs and the most amount of oxygen was found for the PEG-modified SPIONs after reaction with hydrogen peroxide, whereas the least amount of iron was observed for the positively charged SPIONs, more amount of oxygen was observed for the PEG-modified SPIONs and the most amount of iron was observed for the negatively charged SPIONs after reaction with peroxide. The decrease of iron at the surface of samples after reaction with hydrogen peroxide was more in comparison with that of oxygen. This was due to the effect of peroxide on the samples, which caused their surface modification differently.

The results shown in Figure 5 are in coincident with that of Figure 7b that shows that the amount of iron on the surface of positively charged SPIONs decreased more than that of iron on the surface of other SPIONs after the reaction.

As mentioned, we reported the zeta potenital values of TPED-modified and TEPSA-modified SPIONs in our previous works.[18,19] The reduction of zeta potentials of SPIONs after PEG modification was reported, previously.[31,32] More investigation would be required to determine the PEGylation effect of TEPSA-modified SPIONs on their zeta potential values.

It was observed in the current study that the reaction of negatively charged SPIONs with hydrogen peroxide was more rapid than that of PEG-SPIONs and the reaction of this second SPIONs with hydrogen peroxide was more rapid than that of positively charged SPIONs. As the zeta potential value of negatively charged SPIONs was negative, whereas those of PEG-SPIONs and positively charged SPIONs were positive, this indicated that

the negative zeta potential could be more appropriate for the reaction of these nanoparticles with hydrogen peroxide.

The agglomeration of some nanoparticles was not only visible in the TEM images of negatively charge SPIONs, but also it was visible in those of positively charge SPIONs. The colloidal stability of SPIONs can influence their activity with hydrogen peroxide. Further investigation is required to provide information on this issue.

The hydrophilicity/hydrophobicity of nanoparticles could affect their reaction with hydrogen peroxide. The contact angle values of SPIONs with deionized water were measured in our previous work. This study showed no significant hydrophilicity difference of these nanoparticles.[33] Therefore, we conclude that the hydrophilicity of SPIONs could affect their reaction with hydrogen peroxide with the same manner.

The reaction of SPIONs-PEG and negatively charged SPION during the first 30 minutes of the reaction was more rapid than that of positively charged ones with hydrogen peroxide. However, after 30 minutes the rate of the negatively charges SPIONs decreased and attained a plateau more rapidly than the other nanoparticles (Figure 4). This could indicate the rapid consumption of iron from the negatively charges SPIONs in comparison with other nanoparticles. This hypothesis was confirmed with the quantification of iron on the surface of samples with XPS. As seen in Figure 4 and Figure 7b, the amount of iron decreased on the surface of three SPIONs after their reaction with hydrogen peroxide. Moreover, the reaction for negatively charged SPIONs was more rapid that those of other ones (Figure 4) as more amount of iron was observed after the reaction on the suface of these first ones in comparison with the other nanoparticles (Figure 7b). These results were in coincidence with the data in Table 2. As reported in this table, the ratio of Fe-O peak for negatively charged SPIONs before and after reaction with hydrogen peroxide was less than those of other nanoparticles.

The physical and biological properties of some devices were studied, previously.[34-38] Some polymers and nanomaterials were also characterized during recent years.[39,40,41] More investigations are needed to determine the activity of hydrogen peroxide with these devices and materials in conjugation with SPIONs and the possible change in their properties. As hydrogen peroxide is a bacteridical agent with efficient effects on different bacterial

strains,[42-47] its reactivity with these devices and materials could lead to new perspectives of their disinfection.

Some works have been done on the hydrogen peroxide modified materials having various physicochemical, mechanical and biomedical properties.[48-55] No research has been done on the surface properties of the modified materials with SPIONs. Therefore, the analysis of their surface charge and hydrophilicity would be required in order to determine the property change of the modified materials.

The silica shell porosity of SPIONs is important to be investigated as it influences their anchoring with ligands appropriate for MRI or positron emission tomography. Moreover, the MRI contrast enhancement imparted by the nanoparticles requires that there should be intimate contact between water molecules and the iron oxide nanoparticles due to their porous silica shell.[56,57,58] It has been shown that the porosity of silica shell has impact on drug loading and release.[59-62] More work will be necessary to differentiate the role of silica shell porosity of SPIONs or other factors that affect their reactivity with hydrogen peroxide.

CONCLUSIONS

This study verified the reactivity of PEG-modified and functionalized SPIONs with amine and carboxyl groups with hydrogen peroxide in correlation with the physicochemical properties of these nanoparticles. Even though all three SPIONs were capped with silica, the iron surface of SPIONs could react with hydrogen peroxide via the well-known Fenton reaction. Beyond the visibly-observed gas evolution, the reactivity of SPIONs with hydrogen peroxide were characterized by UV-vis kinetics, FTIR and XPS. Our results suggest that the surface properties of the SPIONs can affect their reactivity with hydrogen peroxide. The differences were observed at the oxygen atoms on the surface of SPIONs. Our XPS data revealed that the treatment of these nanoparticles with hydrogen peroxide could affect their surface properties. More investigations would be helpful in the future in order to get more information of the chemical mechanism of the reactivity of hydrogen peroxide with different SPIONs.

ACKNOWLEDGMENTS

We acknowledge the NanoQAM of the Université du Québec à Montréal and the CM^2 laboratory of the École Polytechnique de Montréal for the instruments used for this research.

REFERENCES

(1) Bokobza, L. *J. Appl. Polym. Sci.* **2004**, *93*, 2095. doi:10.1002/app.20684.

(2) Janrao, K. K.; Gadhave, M. V.; Banerjee, S. K.; Gaikwad, D. D. *Asian J. Biomed. Pharmaceut. Sci.* **2014**, *4*, 1. doi:10.15272/ajbps.v4i32.480.

(3) Kucheryavy, P.; He, J.; John, V. T.; Maharjan, P.; Spinu, L.; Goloverda, G. Z.; Kolesnichenko, V. L. *Langmuir* **2013**, *29*, 710. doi:10.1021/la3037007.

(4) Iyer, S. R.; Xu, S.; Strains, J. F.; Bennett, C. H.; Lovering, R. M. *Tissue Eng. B* Rev. **2017**, *23*, 373. doi: 10.1089/ten.TEB.2016.0437.

(5) Lin, M. M.; Kim, D. K.; El Haj, A. J.; Dobson, J. *IEEE Trans Nanobiosci.* **2008**, *7*, 298. doi:10.1109/TNB.2008.2011864.

(6) Mok, H.; Zhang, M. *Expert Opinion on Drug Deliv.* **2013**, *10*, 73. doi:10.1517/17425247.2013.747507.

(7) Zhang, Y.; Kohler, N.; zhang, M. *Biomater.* **2002**, *23*, 1553. doi: 10.1016/s0142-9612(01)00267-8.

(8) Weissleder, R.; Bogdanov, A.; Neuweltb, E. A.; Papisov, M. *Advanced Drug Delivery Reviews* **1995**, *16*, 321. doi:10.1016/0169-409X(95)00033-4.

(9) Bjugstad, K. B.; Redmond, D. E.; Lampe, K. J.; Kern, D. S.; Sladek Jr, J. R.; Mahoney, M. J. *Cell Transplant* **2008**, *17*, 409. doi:10.3727/096368908784423292.

(10) Chan, R. T. H.; Marçal, H.; Russell, R. A.; Holden, P. J.; Foster, L. J. R. *Intern. J. Polymer Sci.* **2011**, *2011*. doi:10.1155/2011/473045.

(11) Park, J. Y.; Daksha, P.; Lee, G. H.; Woo, S.; Chang, Y. *Nanotechnol.* **2008**, *19*, 365603. doi:10.1088/0957-4484/19/36/365603.

(12) Yue-Jian, C.; Juan, T.; Fei, X.; Jia-Bi, Z.; Ning, G.; Yi-Hua, Z.; Ye, D.; Liang, G. *Drug Dev. Ind. Pharm.* **2010**, *36*, 1235. doi:10.3109/03639041003710151.

(13) Laurent, S.; Forge, D.; Port, M.; Roch, A.; Robic, C.; Elst, L. V.; Muller, R. N. *Chem. Rev.* **2008**, *108*, 2064. doi:10.1021/cr068445e.

(14) Barbusinski, K. *Ecol. Chem. Eng.* **2009**, *16*, 347.

(15) Winterbourn, C. C. *Toxicity Lett.* **1995**, *82-83*, 969. doi:10.1016/0378-4274(95)03532-x.

(16) Frenette, M.; Scaiano, J. C. *J. Am. Chem. Soc.* **2008**, *130*, 9634. doi:10.1021/ja801858e.

(17) Wydra, R. J.; Oliver, C. E.; Anderson, K. W.; Dziubla, T. D.; Hilt, J. Z. *RSC Adv.* **2015**, *5*, 18888. doi:10.1039/C4RA13564D.

(18) Stanicki, D.; Boutry, S.; Laurent, S.; Wacheul, L.; Nicolas, E.; Crombez, D.; Elst, L. V.; Lafontaine, D. L. J.; Muller, R. N. *J. Mater. Chem. B* **2014**, *2*, 387. doi:10.1039/C3TB21480J.

(19) Javanbakht, T.; Laurent, S.; Stanicki, D.; Wilkinson, K. J. *Plos One* **2016**, *11*, e0154445. doi:10.1371/journal.pone.0154445.

(20) Cu, Y.; Saltzman, W. M. *Mol. Pharm.* **2009**, *6*, 173. doi:10.1021/mp8001254.

(21) Javanbakht, T.; Laurent, S.; Stanicki, D.; David, E. *J. Appl. Polym. Sci.* **2019**, *136*, 48280. doi:10.1002/app.48280.

(22) Uskoković, V.; Castiglione, Z.; Cubas, P.; Zhu, L.; Li, W.; Habelitz, S. *J. Dent. Res.* **2010**, *89*, 149. doi:10.1177/0022034509354455.

(23) Xu, J.; Xu, C.; Zhao, Y.; Wu, J.; Hu, J. *Front Chem* **2019**, *7*, 831. doi:10.3389/fchem.2019.00831.

(24) Mukherjee, A.; Darlington, T.; Baldwin, R.; Holz, C.; Olson, S.; Kulkarni, P.; DeWeese, T. L.; Getzenberg, R. H.; Ivkov, R.; Lupold, S. E. *Chem. Med. Chem.* **2014**, *9*, 1356. doi:10.1002/cmdc.201300549.

(25) Fessenden, R. W.; Redmon, B. C. *J. Am. Chem. Soc.* **1935**, *57*, 2246. doi:10.1021/ja01314a061.

(26) Killilea, D. W.; Westropp, J. L.; Shiraki, R.; Mellema, M.; Larsen, J.; Kahn, A. J.; Kapahi, P.; Chi, T.; Stoller, M. L. *Plos One* **2015**, *10*, e0128374. doi:10.1371/journal.pone.0128374.

(27) França, R.; Alfa, M.; Olson, N.; Yahia, L'H., Sacher, E. *J. Orthop. Res.* **2017**, *35*, 240. doi:10.1002/jor.23271.

(28) Laurent, S.; Burtea, C.; Thirifays, C.; Häfeli, U. O.; Mahmoudi, M. *Plos One* **2012**, *7*, e29997. doi: 10.1371/journal.pone.0029997.

(29) Kazemzadeh, H.; Ataie, A.; Rashchi, F. *Int. J Modern Phys. Conference Series* **2012**, *5*, 160. doi:10.1142/S2010194512001973.

(30) Namanga, J.; Foba, J.; Ndinteh, D. T.; Yufanyi, D. M. Krause, R. W. M. *J. Nanomater.* **2013**, *2013*, 1. doi:10.1155/2013/137275.

(31) Nazli, C.; Ergenc, T. I.; Yar, Y.; Acar, H. Y.; Kizilel, S. *Int. J. Nanomedicine* **2012**, *7*, 1903. doi:10.2147/IJN.S29442.

(32) Xue, S.; Wang, Y.; Wang, M.; Zhang, L.; Du, X.; Gu, H.; Zhang, C. *Int. J. Nanomedicine* **2014**, *9*, 2527. doi:10.2147/IJN.S59754.

(33) Javanbakht, T.; Laurent, S.; Stanicki, D.; Raphael, W.; Tavares, J. R. *J. Nanoparticle Res.* **2015**, *17*, 462. doi:10.1007/s11051-015-3276-y.

(34) Javanbakht, T.; Ghane-Motlagh, B.; Sawan, M. *Microelectronic Eng.* **2020**, *111305*. doi:10.1016/j.mee.2020.111305.

(35) Ghane-Motlagh, B.; Javanbakht, T.; Shoghi, F.; Wilkinson, K. J.; Martel, R.; Sawan, M. *Mater. Sci. Eng. C* **2016**, *68*, 642. doi:10.1016/j.msec.2016.06.045.

(36) Djavanbakht, T.; Carrier ,V.; André, J.- M.; Barchewitz, R.; Troussel, P. *J. Phys. IV France* **2000**, *10*, 281. doi:10.1051/jp4:20001031.

(37) Tsutsumi, Y.; Niinomi, M.; Nakai, M.; Shimabukuro, M.; Ashida, M.; Chen, P.; Doi, H.; Hanawa, T. *Metals* **2016**, *6*, 76. doi:10.3390/met6040076.

(38) Kiran, A. S. K.; Sireesha, M.; Ramalingam, R.; Kizhakeyil, A.; Verma, N. K.; Lakshminarayanan, R.; Kumar, T. S. S.; Doble, M.; Ramakrishna, S. *J. Mater. Sci.* **2019**, *54*, 13265. doi:10.1007/s10853-019-03811-2.

(39) Javanbakht, T.; Bérard, A.; Tavares, J. R. *Can. J. Chem.* **2016**, *94*, 744. doi:10.1139/cjc-2016-0229.

(40) Javanbakht, T.; David, E. *J. Thermoplastic Composite Mater.* **2020**, 0892705720912767. doi:10.1177/0892705720912767.

(41) Javanbakht, T.; Hadian, H.; Wilkinson, K. J. *J. Engin. Sci.* **2020**, *7*, C1. doi:10.21272/jes.2020.7(1).c1.

(42) Nakajima, T.; Yasuda, H.; Kurita, H.; Takashima, K.; Mizuno, A. *Int. J. Plasma Environ. Sci. Technol.* **2011**, *5*, 42.

(43) Pericone, C. D.; Overweg, K.; Hermans, P. W. M.; Weiser, J. N. *Infect. Immun.* **2000**, *68*, 3990. doi:10.1128/iai.68.7.3990-3997.2000.

(44) Hernandez, P.; Sager, B.; Fa, A.; Liang, T.; Lozano, C.; Khazzam, M. *Bone Joint Res.* **2019**, *8*, 3. doi:10.1302/2046-3758.81.BJR-2018-0145.R1.

(45) Ríos-Castillo, A. G.; González-Rivas, F.; Rodríguez-Jerez, J. J. *J. Food Sci.* **2017**, *82*, 2351. doi:10.1111/1750-3841.13790.

(46) Brudzynski, K.; Abubaker, K.; St-Martin, L.; Castle, A. Front Microbiol. **2011**, *2*, 1. doi:10.3389/fmicb.2011.00213.

(47) Samoĭlenko, I. I.; Vasil'eva, E. I.; Pavlova, I. B.; Tumanian, M. A. *Zh. Mikrobiol. Epidemiol. Immunobiol.* **1983**, *12*, 30.

(48) Lai, Y.; He, S.; Luo, S.; Bi, W.; Li, X. R.; Sun, C.; Seshan, K. *Catalytic Processes Mater. Faculty Sci. Technol.* **2015**, *69*, 39. doi:10.1016/j.catcom.2015.05.019.

(49) Zhang, C.; Li, R.; Liu, J.; Guo, S.; Xu, L.; Xiao, S.; Shen, Z. *Cermaics International* **2019**, *45*, 13385. doi:10.1016/j.ceramint.2019.04.035.

(50) Shen, B.; Lieu, Z.; Xu, H.; Wang, F. *Fuel* **2019**, *235*, 878. doi:10.1016/j.fuel.2018.08.082.

(51) Zhou, G.; Yao, Y.; Lu, Z.; Yang, X.; Han, J.; Wang, G.; Rao, X.; Li, P.; Liu, Q.; Song, Q. *Nanotechnol.* **2017**, *28*, 425202. doi:10.1088/1361-6528/aa8397.

(52) Liu, Y.; Cao, Z. *Energy Procedia* **2011***, 11*, 3239. doi:10.1016/j.egypro.2011.10.678.

(53) Haberland, A.; Mäder, K.; Stößer, R.; Schimke, I. *Agents Actions* **1993**, *40*, 166. doi:10.1007/BF01984056.

(54) Wu, J. M.; Wang, M.; Hayakawa, S.; Tsuru, K.; Osaka, A. **2006**, *309-311*, 407. doi:10.4028/www.scientific.net/kem.309-311.407.

(55) Ariyanto, T.; Sarwendah, R. A. G.; Amimmal, Y. M. N.; Laksmana, W. T.; Prasetyo, I. *Processes* **2019**, *7*, 835. doi:10.3390/pr7110835.

(56) Patel, D.; Kell, A.; Simard, B.; Deng, J.; Xiang, B.; Lin, H.- Y.; Gruwel, M.; Tian, G. *Biomaterials* **2010**, *31*, 2866. doi:10.1016/j.biomaterials.2009.12.025.

(57) Zhang, L.; Wang, Y.; Tang ,Y.; Jiao, Z.; Xie, C.; Zhang, H.; Gu, P.; Wei, X.; Yang, G.- Y.; Gu, H.; Zhang, C. *Nanoscale* **2013**, *5*, 4506. doi:10.1039/c3nr00119a.

(58) Zhang, J.; Rosenholm, J. M.; Gu, H. *Chemphyschem.* **2012**, *13*, 2016. doi:10.1002/cphc.201100943.

(59) Wang, C. F.; Sarparanta, M. P.; Mäkilä, E. M.; Hyvönen, M. L. K.; Laakkonen, P. M.; Salonen, J. J.; Hirvonen, J. T.; Airaksinen, A. J.; Santos, H. A. *Biomaterials* **2015**, *48*, 108. doi:10.1016/j.biomaterials.2015.01.008.

(60) Martín-Palma, R. J.; Hernández-Montelongo, J.; Torres-Costa, V.; Manso-Silván, M.; Muñoz-Noval, Á. *Expert Opin. Drug Deliv.* **2014**, *11*, 1273. doi:10.1517/17425247.2014.919254.

(61) Chen, Y.- C.; Huang, X.- C.; Luo, Y.- L.; Chang, Y.- C.; Hsieh, Y.- Z.; Hsu, H. *Sci. Technol. Adv. Mater.* **2013**, *14*, 044407. doi:10.1088/1468-6996/14/4/044407.

(62) Bharti, C.; Nagaich, U.; Pal, A. K.; Gulati, N. *Int. J. Pharm. Investig.* **2015**, *5*, 124. doi:10.4103/2230-973X.160844.

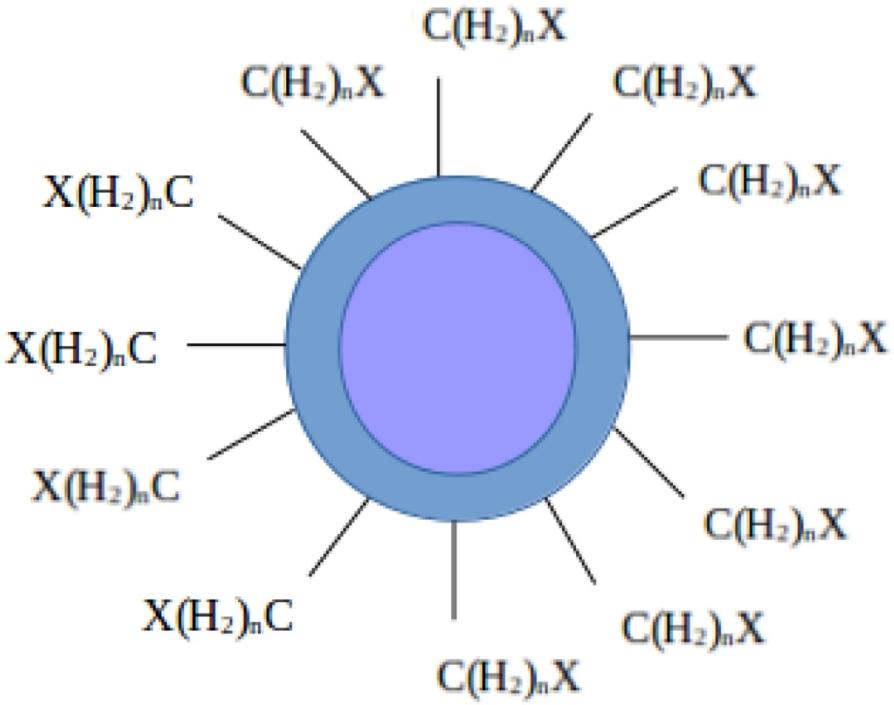

Figure 1

124x99mm (300 x 300 DPI)

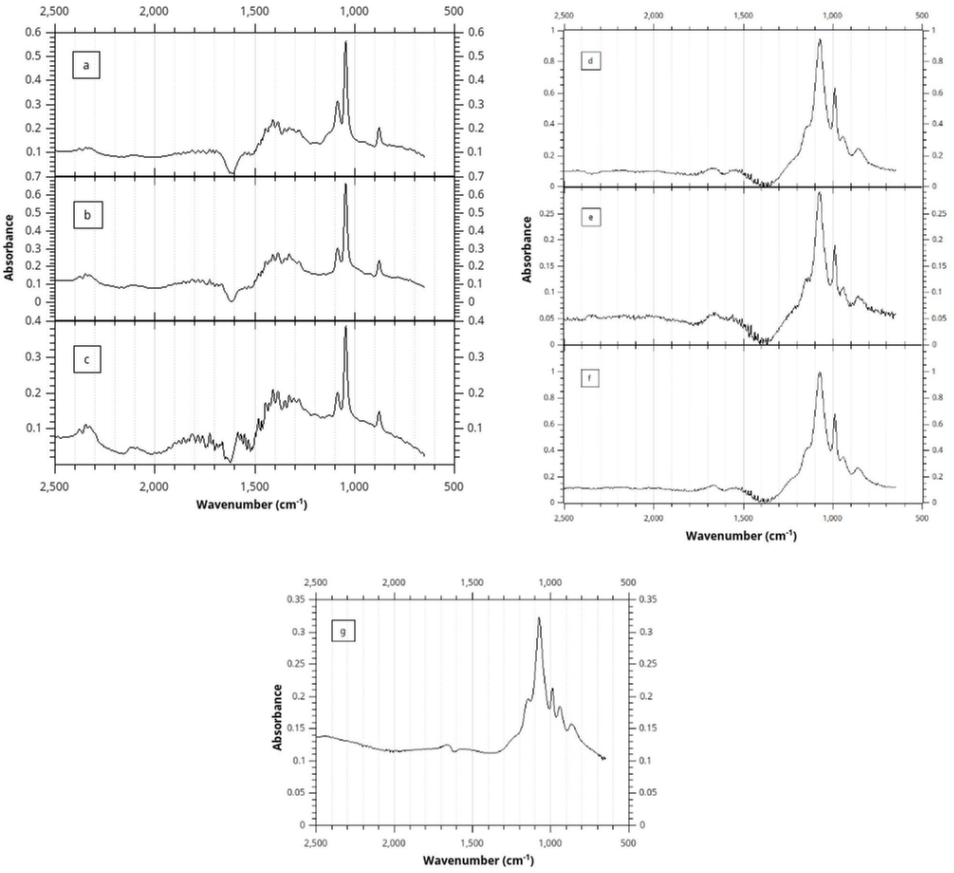

Figure 2

89x85mm (300 x 300 DPI)

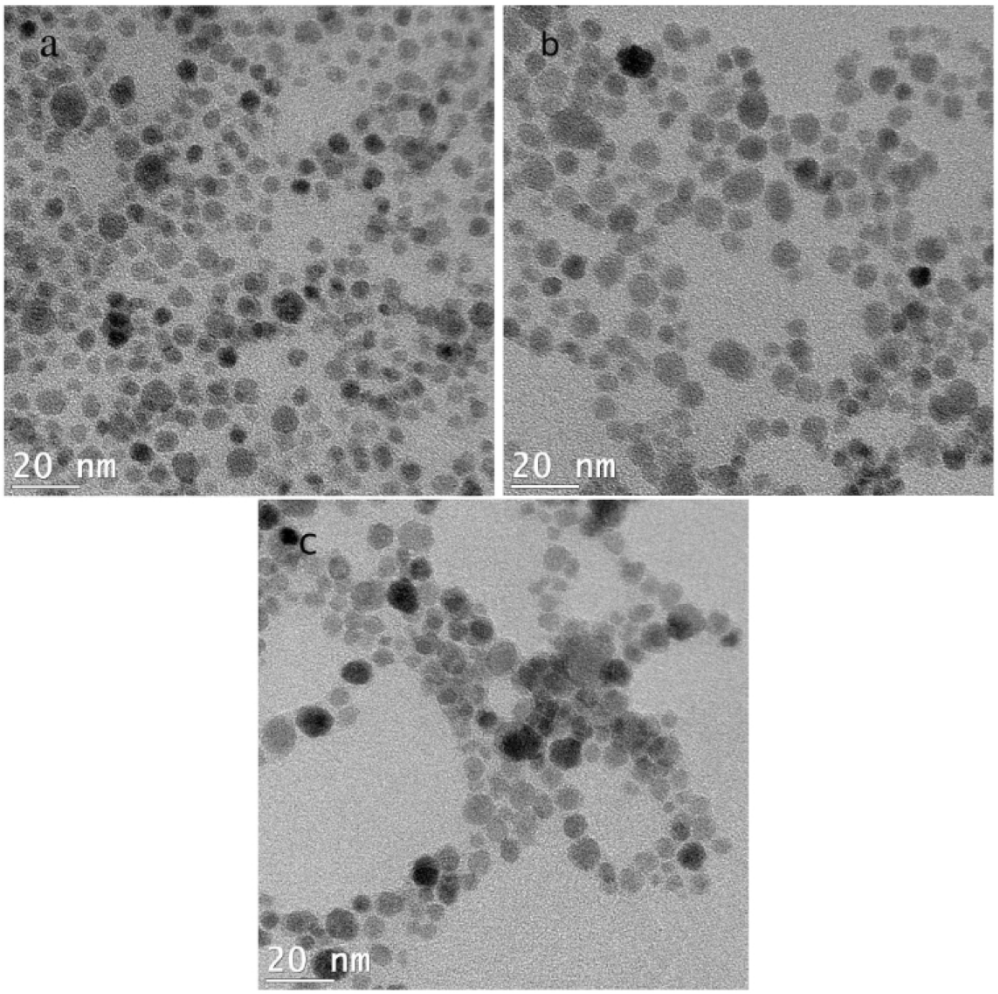

Figure 3

200x199mm (300 x 300 DPI)

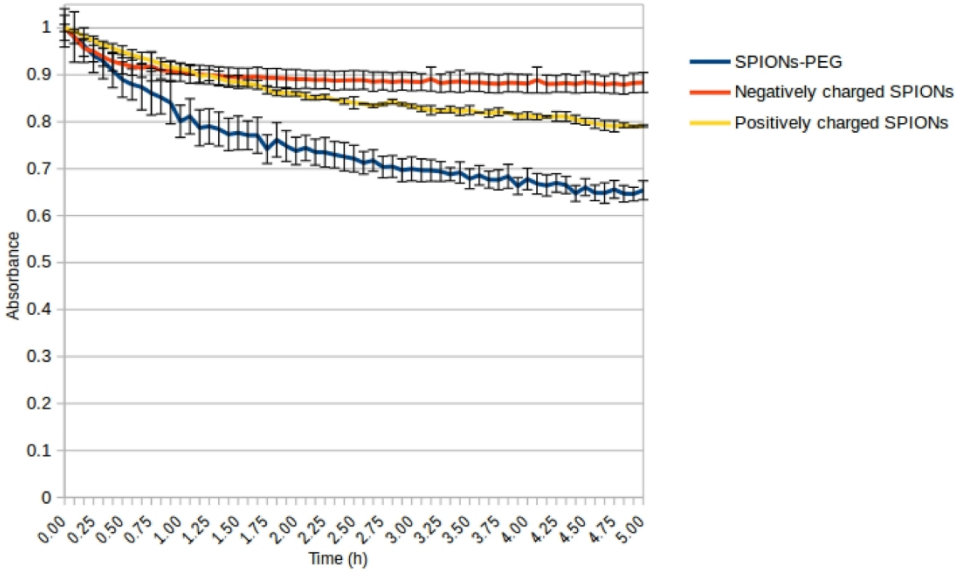

Figure 4

196x114mm (300 x 300 DPI)

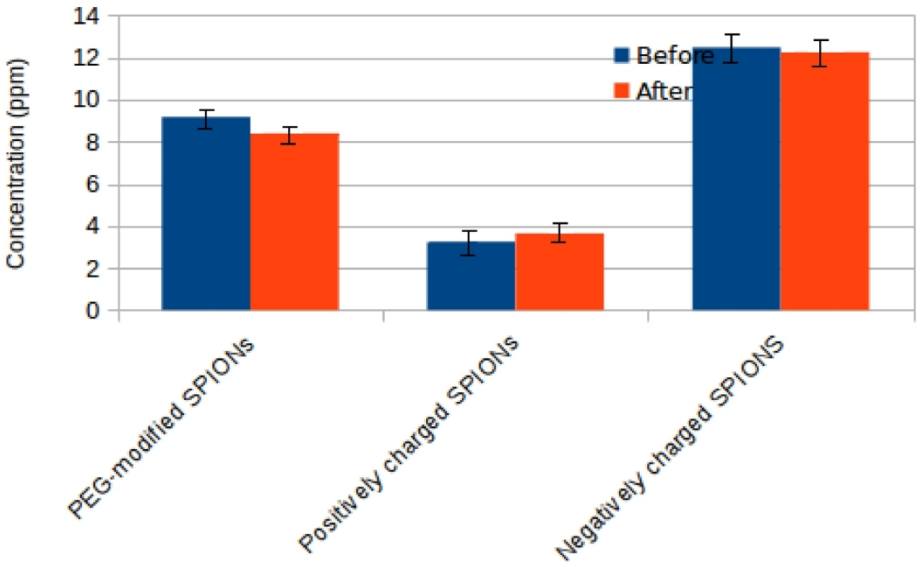

Figure 5

186x111mm (300 x 300 DPI)

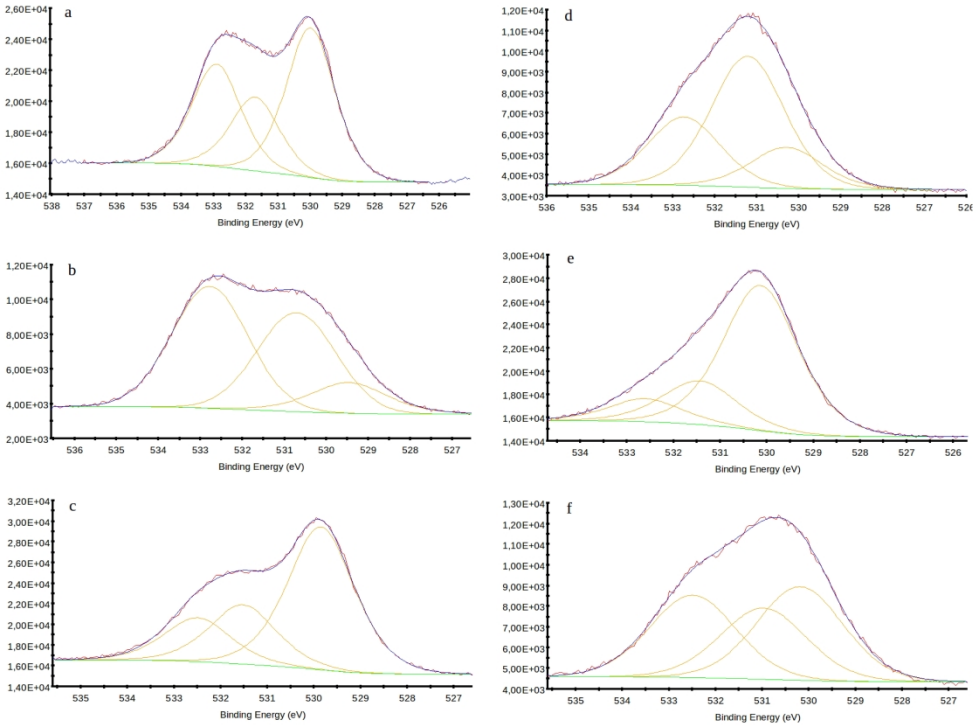

Figure 6

529x397mm (300 x 300 DPI)

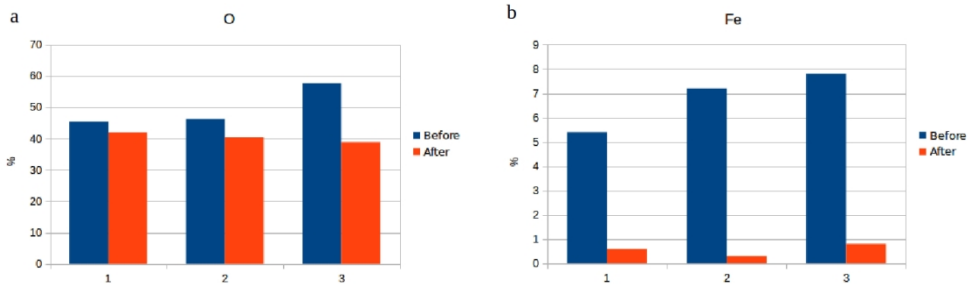

Figure 7

406x124mm (300 x 300 DPI)